DOES THE FIR-RADIO CORRELATION EVOLVE WITH REDSHIFT IN IRREGULAR AND DISK GALAXIES?

M. S. Pavlović[1,2]

[1]*Mathematical Institute of the Serbian Academy of Sciences and Arts*
Kneza Mihaila 36, 11000 Belgrade, Serbia

[2]*Faculty of Mathematics, Department of Astronomy, University of Belgrade*
Studentski Trg 16, 11000 Belgrade, Serbia

E–mail: *marinap@mi.sanu.ac.rs*

SUMMARY: It was confirmed that there is a strong linear correlation between the thermal far-infrared (FIR) and non-thermal radio emission of the star-forming galaxies. Recent works based on this correlation over large redshifts have shown that the correlation is evolving towards higher redshifts. In this paper, possible physical causes that lead to the evolution of this correlation are explored. One possible cause is that the interaction between galaxies is responsible for this behavior. We used the morphology of galaxies, as an indicator of past or present interactions, because it is generally known that the irregular morphology of galaxies is a consequence of collisions or close approaches. To test this hypothesis, a sample of dusty star-forming galaxies up to a redshift $z = 3.5$ from the COSMOS field has been selected. The sample has been divided, according to the morphological type, into two subsamples (disk and irregular galaxies), and the evolution of the correlation with redshift has been analyzed separately for both of them. It was found that in both subsamples there is no indication for the redshift evolution of the FIR-radio correlation. However, it was also found that the mean correlation parameter, q_{FIR}, is lower in irregular galaxies, which may indicate that they can still affect the evolution of the correlation if their abundance in the sample increases towards higher redshifts. Disk galaxies, which statistically dominate the sample, may be responsible for the lack of this evolution. On the other hand, a fundamental problem with optically determined morphology is the dust obscuration in massive galaxies at $z > 2$. To test the idea that interacting galaxies are responsible for redshift evolution of the FIR-radio correlation, it is, necessary to analyze a much larger sample for which the morphology has been determined, taking into account the VLA and ALMA imaging in addition to optical images, and which contains a higher fraction of irregular galaxies. Finally, it was also found that the q_{FIR} parameter and its evolution are very sensitive to the radio spectral index above $z > 1$ and that its misinterpretation and taking a constant value of $\alpha = 0.7$ may be responsible for the observed evolution of the correlation.

Key words. Cosmic rays − Galaxies: interactions − Galaxies: evolution − Radio continuum: galaxies − Infrared: galaxies

1. INTRODUCTION

Observations have shown that there is a robust linear relationship between the radio and the far-infrared emission in the star-forming galaxies (van der Kruit 1971, Helou et al. 1985, Condon et al. 1991, Yun et al. 2001, Bell 2003, Sargent et al. 2010, Delhaize et al. 2017, Gürkan et al. 2018, Molnár et al. 2018, Algera et al. 2020, Delvecchio et al. 2021), named the Far-infrared radio correlation (FIRC). The origin of this correlation probably stems from the formation and death of massive stars. Through UV radi-

ation, young massive stars are the only heating source for interstellar dust, which then emits the thermal infrared emission. Several million years after these massive stars exploded as supernovae, their remnants become the source of cosmic rays, which then emit the non-thermal radiation through the acceleration of relativistic electrons in shock waves (Condon et al. 1991).

Due to its stability, FIRC has found many applications in astrophysics. It is used as a tool for identification of radio-loud active galactic nuclei (AGNs) (Donley et al. 2005, Norris et al. 2006, Park et al. 2008, Del Moro et al. 2013), and for distance estimations of high redshift galaxies (Condon 1992, Bell 2003, Murphy et al. 2012). One of the most important applications of the FIRC is in the use of radio luminosity as a tracer of the Star Formation Rate (SFR) (Condon 1992, Bell 2003, Murphy et al. 2012). The FIRC is defined via the ratio parameter 1:

$$q_{FIR} = \log\left(\frac{F_{\mathrm{FIR}}}{3.75 \times 10^{12} \mathrm{Wm}^{-2}}\right) - \log\left(\frac{S_{1.4}}{\mathrm{Wm}^{-2}\mathrm{Hz}^{-1}}\right) \quad (1)$$

where $S_{1.4}$ and F_{FIR} are the rest frame radio emission flux density at 1.4 GHz and the rest-frame far-infrared emission flux density from $42\mu m$ to $122\mu m$, respectively (Helou et al. 1985). Observations of star-forming galaxies in the local universe have shown that the value of this parameter is $q_{\mathrm{FIR},0} = 2.34 \pm 0.01$ (Yun et al. 2001). However, recent observations of 12000 star-forming galaxies up to the redshift $z < 6$, in the COSMOS field, have revealed that this parameter evolves, specifically, that it decreases with redshift as $q_{\mathrm{FIR}}(z) = (2.52 \pm 0.03)(1 + z)^{-0.21 \pm 0.01}$ (Delhaize et al. 2017). Several physical processes have been proposed to explain the evolution of FIRC with redshift. The most important one is a possible contamination by the presence of AGNs (Magnelli et al. 2010, Sajina et al. 2008) as we still do not have solid criteria for their exclusion from higher redshifts or a considerable contribution of thermal radio emission (Delhaize et al. 2017). Another possibility is the contamination by major mergers at high redshifts (Pavlović et al. 2019), which will further be investigated in this work. It is known so far that the galactic merger rate increases up to redshifts $z \approx 2-3$ (Mortlock et al. 2013, Mundy et al. 2017, Ventou et al. 2017). Some of the previous works have shown that the major mergers between galaxies can lead to enhanced non-thermal radio emission: through an additional synchrotron emission from gas bridges in taffy-like systems (Murphy 2013), through amplification of magnetic fields (Kotarba et al. 2010), or through acceleration of cosmic rays in tidal shocks that develop in the interstellar medium of interacting galaxies (Donevski and Prodanović 2015, Prodanović et al. 2013). In our previous work (Pavlović et al. 2019), we presented theoretical models of the FIR-radio correlation shape depending on the share of the so-called peculiar (irregular and interacting) galaxies, and of

interacting galaxies separately (as shown in Fig. 1 and 2 in this paper). It is important to mention that we took the fraction of peculiar galaxies and the function of their evolution with redshift from the paper Mortlock et al. (2013). Most of the interaction-based models presented in this paper show a decreasing correlation parameters towards higher redshifts which is consistent with what was found by Delhaize et al. (2017). On the other hand, the models that include all peculiar galaxies, including the irregular galaxies that are thought to be the result of past collisions, show a significant evolution of the FIR-radio correlation with redshift, that is, a decrease in the correlation parameter. Inspired by this result, we decided to examine the evolution of the FIR-radio correlation with redshift on a larger sample of submillimeter galaxies (SMGs).

The influence of the morphology on the evolution of FIRC was also examined up to a redshift $z \approx 1.5$ in a recent paper by Molnár et al. (2018) who showed that, in spheroid-dominant galaxies (mainly elliptical and disk galaxies with a prominent bulge component) there is a decrease of the correlation parameter with redshift and that in the case of disk-dominant galaxies (spiral/disk galaxies and irregular galaxies), the evolution of correlation is small. The main difference that will be introduced in this paper is in the morphology of galaxies itself. As this paper relies on the hypothesis that the interaction between galaxies is responsible for the observed evolution of the correlation, we will pay special attention to the irregular morphological type of galaxies. On the other hand, it is considered that the cause of the correlation is the formation of stars in galaxies, we decided to exclude elliptical galaxies from the sample because they are passive and have long since completed the phase of star formation (Chiosi and Carraro 2002, De Lucia et al. 2006). Furthermore, we increased the range of the redshift up to $z = 3.5$ relative to $z = 1.5$ in Molnár et al. (2018) because the frequency of interactions between galaxies is also thought to increase up to this redshift (Mortlock et al. 2013, Mundy et al. 2017, Ventou et al. 2017). Since, after the redshift $z = 1$, the determination of the morphology of galaxies based on the optical images is very imprecise, especially for the dust-obscured systems we are currently working with, we decided to use three morphological catalogs for this purpose. A detailed principle for morphology determination of galaxies will be described in Section 2.

This paper is organized as follows: Section 2 contains a detailed analysis of the data, such as determining the morphology of galaxies, explaining the criteria used to reject AGNs. Section 3 is dedicated to the spectral energy distribution curve (SED) fitting, as well as to calculating the spectral indices. This chapter also contains references to all the catalogs used in this paper. In Sections 4 and 5, I presented the results and discussion, respectively.

2. DATA ANALYSIS

In order to examine the evolution of the FIR-radio correlation with the redshift found in Delhaize et al. (2017), we used a SMGs over the 2deg^2 COSMOS field, that has both radio and infrared observations. The chosen SMGs were discovered by the $\lambda_{obs} = 1.1$ mm blank-field continuum survey over an area of 0.72 deg^2 or 37.5% of the entire 2deg^2 COSMOS field, conducted with the AzTEC bolometer array on the 10m Atacama Submillimeter Telescope Experiment (Ezawa et al. 2004). The angular resolution of these observations was 34″ FWHM. Because of the source-deblending from the older generation single-dish telescope (Casey et al. 2014, Pearson et al. 2017, Hurley et al. 2017, Donevski et al. 2018, Wang 2019), the contribution of many sources will significantly affect the estimation of the FIR luminosities. In these cases, the q_{FIR} parameter will be the upper limit for the observed source.

2.1. Morphology

Several morphological catalogues cover the COSMOS field, including the Tasca, Cassata, and Zurich catalogs (Tasca et al. 2009, Cassata et al. 2007, Scarlata et al. 2007, Sargent et al. 2007), that were used in this paper. Each catalogue provides a morphological classification of galaxies into different types (rather than just morphology-related parameters), and all objects are classified as 1-early type, 2-disk (spiral), and 3-irregular galaxies.

To obtain a morphological type for each of our sources, I used a ladder approach: if the source is classified as an irregular/disk in each of the three catalogs, I classified the source as an irregular/disk, and if two out of the three catalogs gives the same morphology, this most common class is adopted. Furthermore, we purified the sample by excluding all galaxies classified as early-type because they are not relevant to this research. Although the morphology of galaxies could be more precise, as I mentioned in the Section 1, in order to avoid the introduction of another model-dependent parameter, I have decided to adopt an already defined morphology.

2.2. AGN selection and exclusion

Active galactic nuclei show a prominent radio emission of non-thermal nature, which could significantly influence the evolution of FIRC, as the nature of the non-thermal radio emission is not the same as in star-forming galaxies. On the other hand, it is known that the distribution of AGN (quasars) reaches a maximum at the redshift $z = 2$ (Croom et al. 2001, 2004), which means that they must be removed from the sample we are observing. In order to clean the sample from the active galactic nuclei, I used the COSMOS VLA 3GHz AGN Catalog (Smolčić et al. 2017a) where the AGNs were iden-

tified using 4 criteria in different parts of the spectrum (mid-infrared, X, and radio domain) (Donley et al. 2012, Elvis et al. 2009, Civano et al. 2012, 2016, Marchesi et al. 2016, Smolčić et al. 2017a, Delvecchio et al. 2014). Exact details on the AGN selection can be found in Delvecchio et al. (2017). We cross-referenced our sample with the COSMOS VLA 3GHz AGN Catalog and discarded every object that showed the presence of AGN by any criteria. Although using these criteria we are sure that there is no contamination from AGNs in the sample, there is a possibility that we lose the star-forming sources with excess radio emission but without the presence of AGN. This can result in a reduction of our sample, because these are the sources that are of interest to us, which, on the other hand, could mask the evolution of the correlation, i.e. the excess of the radio emission towards higher redshifts.

2.3. Photometric and spectroscopic redshift

To study the evolution of the Far-infrared radio correlation, it was required that each object in the sample has a redshift. Spectroscopic redshifts are available in the COSMOS spectroscopic redshift master catalog (Salvato et al. in prep), which were measured in the VUDS survey (Le Fèvre et al. 2015, Tasca et al. 2017), zCOSMOS survey (Lilly et al. 2007), and DEIMOS runs (Capak et al. in prep.), and are highly reliable. For objects where the spectroscopic redshift was unavailable, a photometric redshift from the COSMOS2015 photometric redshift catalog (Laigle et al. 2016) was used.

The histograms below show the distribution of photometric (blue) and spectroscopic (pink) redshifts of galaxies in the COSMOS field, for disk (left) and irregular (right) galaxies. As we can see, the photometric redshifts dominate the sample. For most of the galaxies that have a spectroscopic redshift, we also have a photometric one. The differences are generally $z_s \approx z_p 0.5$ (where z_p and z_s are photometric and spectroscopic redshift, respectively), which would introduce an additional error in the results. Therefore, a decision was made to use spectroscopic redshifts for all the objects for which it is available, in our case it is for 33 disk and 11 irregular galaxies, respectively. For the rest of the sample, a photometric redshift was provided.

3. SED MODELING OF THE FIR DATA AND RADIO-SELECTED SAMPLE

In order to obtain the total FIR flux density, we have used infrared observations in the following bands: $24\mu m$, $100\mu m$, $160\mu m$, and $250\mu m$, $350\mu m$ and $500\mu m$ data taken from the Herschel continuum observations (Pilbratt et al. 2010) and obtained as a part of the Photodetector Array Camera and Spectrometer (PACS) Evolutionary Probe (Lutz et al. 2011, PEP) and the Herschel Multi-tiered Extra-
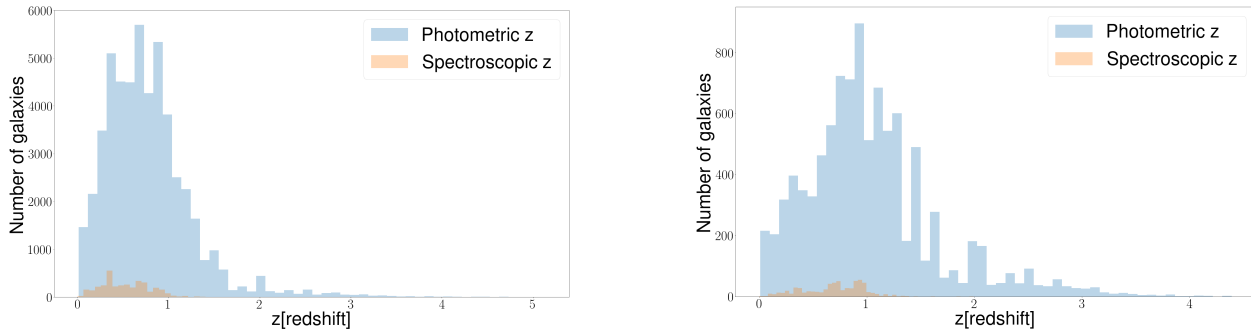
Fig. 1: The distribution of disk galaxies (left) and irregular galaxies (right) depending on the redshift for all galaxies from the COSMOS field that have defined the morphology. Blue and pink colors represent objects that have photometrically and spectroscopically obtained redshifts, respectively.

galactic Survey (Oliver et al. 2012, HerMES) programs. Next, the SED curve was fitted on those points by a second-degree polynomial for each galaxy separately. The total FIR flux density was then obtained by integrating the SED curve in the rest frame in the range of $42\mu m$ to $122\mu m$. To check whether such fitting of the SED curve introduces a significant error when calculating the FIR luminosity, we used the sample AzTEC/ASTE published in the paper (Miettinen et al. 2017) on which we performed a similar analysis as presented in this paper and came to the conclusion that FIR luminosities can be distinguished by $100\mu Jy$, which is an order of magnitude smaller than the instrumental error we get at these wavelengths. On the other hand, this difference will introduce a dispersion in the q_{FIR} parameter of only 0.03, which is again an order of magnitude smaller from its standard deviation, so we decided that the use of the second-degree polynomial fit in the FIR wavelengths is a good approximation.

Primarily, flux densities of two wavelengths in the radio domain were used to calculate the spectral indices for given galaxies. We used the 3 GHz integrated radio flux density from the COSMOS VLA 3GHz Multiwavelength Counterpart Catalog (Smolčić et al. 2017b), and the 1.4 GHz radio flux density from the COSMOS VLA Deep Catalog (Schinnerer et al. 2010, Aretxaga et al. 2011). The spectral index was calculated assuming a power-law spectrum with index α where $S_\nu \propto \nu^\alpha$ of radio sources by comparing the 3 GHz fluxes to those in the 1.4 GHz VLA COSMOS data. For those galaxies with flux at 1.4 GHz, the rest-frame, k-corrected, flux densities have been calculated using the previously determined spectral index (Magnelli et al. 2015) at 1.4 GHz and were used for determining the q_{FIR} parameter. For the rest of the sample, we converted the observer-frame 3 GHz fluxes into 1.4 GHz luminosities:

$$L_{1.4GHz} = \frac{4\pi D_L^2}{(1+z)^{\alpha+1}} \left(\frac{1.4}{3}\right)^\alpha S_{3GHz} \qquad (2)$$

where D_L is the luminosity distance to the object in meters. $L_{1.4GHz}$ and S_{3GHz} are the observed radio luminosity at 1.4 GHz and observed flux density at 3 GHz, respectively. For all physical quantities used in this paper, the errors were propagated and combined in quadrature.

Eq. (2) tells us that we need a radio spectral index to switch the luminosity from the observed to rest frame. In cases where we do not have flux densities at two wavelengths in the radio domain, a fixed value of this parameter was used. Therefore, I wanted to examine whether one value of the spectral index taken for the rest of the sample will significantly affect the results. Fig. 2 shows the dependence of the correlation parameter on the redshift for fixed spectral index $\alpha = -0.6$ (green circles), $\alpha = -0.7$ (red exes), $\alpha = -0.8$ (burgundy triangles) and $\alpha = -0.9$ (purple rectangles). We can see that, as we move towards larger redshifts, the value of the spectral index significantly affects the value of the correlation parameter:

$$q_{FIR} = \log\left(\frac{F_{FIR}(1+z)^{(1+\alpha)}}{\left(\frac{1.4}{3}\right)^\alpha S_{3GHz}}\right) \qquad (3)$$

where, already at redshift 1.5, the value of the correlation parameter changes from $q_{-0.9} = 2.21$ to $q_{-0.6} = 2.42$. This means that taking a constant value of the radio spectral index automatically pulls the natural evolution of the correlation parameter toward higher redshifts. On the other hand, the steeper radio spectral index used in previous research ($\alpha = -0.7$, Delhaize et al. (2017)) will result in lower values of the correlation parameter, which may be responsible for the evolution of the correlation with redshift itself. The recent research (Klein et al. 2018) has shown that the radio spectral index in SMG galaxies is not as steep as previously thought, rather, it is closer to $\alpha = -0.56$, which gives a higher value of the correlation parameter compared to previous analyzes. All this leads to the conclusion that taking a constant value of this parameter, especially steeper values, can lead to the apparent evolution of the FIR-radio correlation.
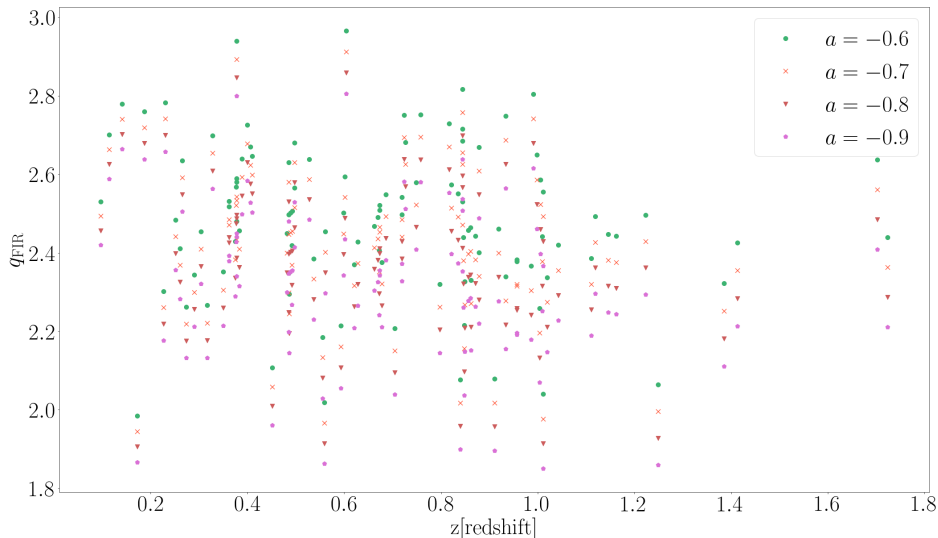
Fig. 2: Dependence of the correlation parameter on redshift for different spectral indices: $\alpha = -0.6$ (green circles), $\alpha = -0.7$ (red exes), $\alpha = -0.8$ (burgundy triangles) and $\alpha = -0.9$ (purple rectangles).

For 109 galaxies from the sample, that does not have a flux density at two wavelengths in the radio domain, a fixed spectral index $\alpha = -0.59 \pm 0.20$ (Klein et al. 2018) was assumed, which is a big difference from the work Delhaize et al. (2017), where they took $\alpha = -0.7$. This difference may be responsible for the divergence of our results from the previously observed evolution of the correlation, as seen in Section 4.

After determining the morphology, removing the AGNs, and cleaning the sample, the final sample consists of 159 disks and 44 irregular galaxies. In order to get a larger sample and statistically more significant results, galaxies from previous work were added to this sample (Pavlović et al. 2019), so the final sample used in this paper consists of 236 galaxies, 181 of which are disk and 55 are irregular.

4. RESULTS

In order to compare this work to our previous work (Pavlović et al. 2019) where we had a lack of galaxies at a redshift $z < 1$, an analysis was performed on the entire sample from $0 < z < 3.5$ but also on the $z > 1$ subsample. We determined the mean value of the correlation parameter for the entire sample of galaxies to be $q_{\mathrm{FIR}} = 2.34 \pm 0.30$, and for galaxies at redshift $z > 1$ where we get $q_{\mathrm{FIR}(z>1)} = 2.21 \pm 0.36$. Furthermore, we determined the mean value of the correlation parameter separately for each of the subsamples, which is $q_{\mathrm{FIR}} = 2.34 \pm 0.30$ and $q_{\mathrm{FIR}} = 2.19 \pm 0.34$, for disk and irregular galaxies, respectively. In addition, we determine the median value with 16th and 84th percentile for q_{FIR} for disk and irregular galaxies separately and the results are summarised in Table 1 for two different ranges of stellar masses $10.5 < \log(M_*/M_o) < 10.5$,

Table 1: Median values for q_{FIR} with 1σ deviations for disk and irregular galaxies seperatly, for two different ranges of stellar masses.

Disk galaxies	Irregular galaxies
$log(M_*/M_0) < 10.5$	
$q_{-1\sigma} = 2.19$	$q_{-1\sigma} = 1.97$
$q_{\mathrm{median}} = 2.46$	$q_{\mathrm{median}} = 2.21$
$q_{+1\sigma} = 2.65$	$q_{+1\sigma} = 2.42$
$log(M_*/M_0) > 10.5$	
$q_{-1\sigma} = 2.15$	$q_{-1\sigma} = 1.93$
$q_{\mathrm{median}} = 2.38$	$q_{\mathrm{median}} = 2.34$
$q_{+1\sigma} = 2.56$	$q_{+1\sigma} = 2.53$

in order to compare the results with Delvecchio et al. (2021).

As we can see, both the mean and median q_{FIR} parameters show lower values in the sample of irregular galaxies, and are consistent with the possibility that those galactic collisions might be driving the evolution of q_{FIR} towards higher redshift, as was also pointed out in the previous works of Donevski and Prodanović (2015), Pavlović et al. (2019).

In order to compare the results with previous papers (Delhaize et al. 2017, Pavlović et al. 2019), the dependence of the correlation parameter with redshift was examined in the form of $q_{\mathrm{FIR}}(z) = a(1 + z)^b$, where a is a fitting constant and b is a degree coefficient, for two different morphological types separately.

Fig. 3 shows the dependence of $q_{\mathrm{FIR}}(z)$ defined previously for 181 disk galaxies (left), and 55 irregular galaxies (right). The red dashed and dash-dotted lines represent power-low fits $q_{\mathrm{FIR}} = (2.4 \pm 0.01)(1 +$
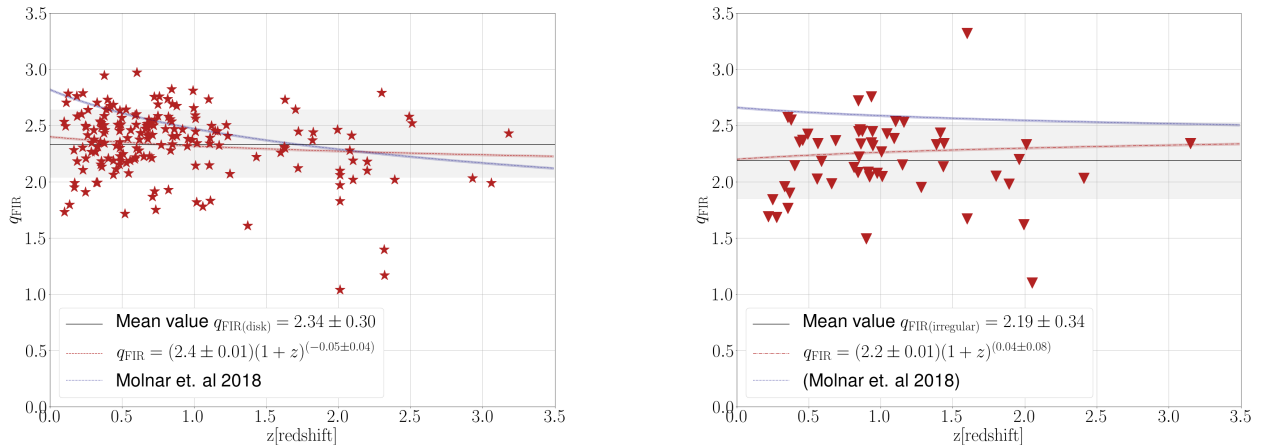
19

Fig. 3: q_{FIR} as a function of redshift. Left: data for disk galaxies (red stars) were fitted with the red dashed line. Right: data for irregular SMGs (red triangles) were fitted with a red dash-dotted line. The solid black line is the mean value for the q_{FIR} parameter with the grey-shaded region representing its standard deviation for disk (left) and irregular (right) galaxies. Blue lines represent the results from Molnár et al. (2018) for spheroid-dominated (left) and disk-dominated (right) galaxies, for comparison.

$z)^{(-0.05\pm0.04)}$ and $q_{FIR} = (2.2 \pm 0.1)(1 + z)^{(0.04\pm0.08)}$, for disk and irregular galaxies, respectively. Blue lines represent the results from Molnár et al. (2018) for spheroid-dominated (left) and disk-dominated (right) galaxies, for comparison. Although trends in different morphological types appear to be opposing, both are consistent within errors with no evolution with redshift. However, it is important to note that small statistics and large uncertainties especially at redshifts $z > 1$, might be obscuring any underlying evolution found by Delhaize et al. (2017). Another existing explanation of the discrepancy of our results with Delhaize et al. (2017) is that the observed evolution of the FIR-radio correlation with redshift does not exist and that it is the result of poor estimation of the spectral index in star-forming galaxies in the young universe.

Furthermore, I analyzed the dependence of the correlation parameter of redshift for the entire sample (disk + irregular) of 236 galaxies. The fitting results are shown in Fig. 4. The solid blue curve represents a power-low fit for the whole sample of 236 galaxies in the shape of $q_{FIR} = (2.4 \pm 0.01)(1 + z)^{(-0.02\pm0.03)}$. The whole sample does not show any indications for the evolution of the redshift correlation, as well. Fig. 4 also shows the previously observed trend found by Delhaize et al. (2017), as an orange dotted line, for easy comparison.

As we can see in Fig. 4, the number of points on the highest redshift bin is significantly lower than on the small redshifts, which may mean that this small number of data points overlaps the actual value of the correlation parameter in these stages. On these redshift bins, outliners are not weighted, and the number of data points is exclusively a consequence of the undefined (or non-inclusively defined) morphology of

galaxies. On the other hand, the value of the correlation parameter at these redshifts does not exceed the standard deviation of the nominal value (Yun et al. 2001), so I decided that there was no need to remove the outliners.

A recent paper (Delvecchio et al. 2021) has shown that the infrared radio correlation shows a significant evolution with stellar mass (M_*) while a weaker dependence on redshift has been found. It was found that the correlation parameter q_{IR} shows lower values in galaxies of higher stellar masses. As our sample also showed a weak dependence of the correlation on the redshift, we decided to check whether the correlation with the redshift would occur for different bins of stellar masses. Stellar masses were also taken from the COSMOS2015 photometric redshift catalog (Laigle et al. 2016), and the dependence of the correlation parameter was analyzed for 4 bins of stellar masses: $\log(M_*/M_o) < 10$, $10 < \log(M_*/M_o) < 10.5$, $10.5 < \log(M_*/M_o) < 11$, and $\log(M_*/M_o) > 11$.

In contrast to the work Delvecchio et al. (2021), in our sample for three bins of stellar masses, we did not find any sign of the evolution of correlation when fitting errors are taken into account, except for galaxies with stellar masses $10.5 < \log(M_*/M_o) < 11$, where the correlation parameter shows evolution with redshift in the form of: $q_{FIR}(z) = (2.5 \pm 0.1)(1 + z)^{(-0.11\pm0.05)}$. The apparent independence of the correlation parameter from the stellar mass can be explained by a statistically small sample with respect to work Delvecchio et al. (2021). On the other hand, massive galaxies do originate from the collision of more galaxies and, in the past, unlike less massive galaxies, have experienced a number of close approaches (Conselice 2007, Conselice et al. 2009, Bertone and Conselice 2009), which can contribute to
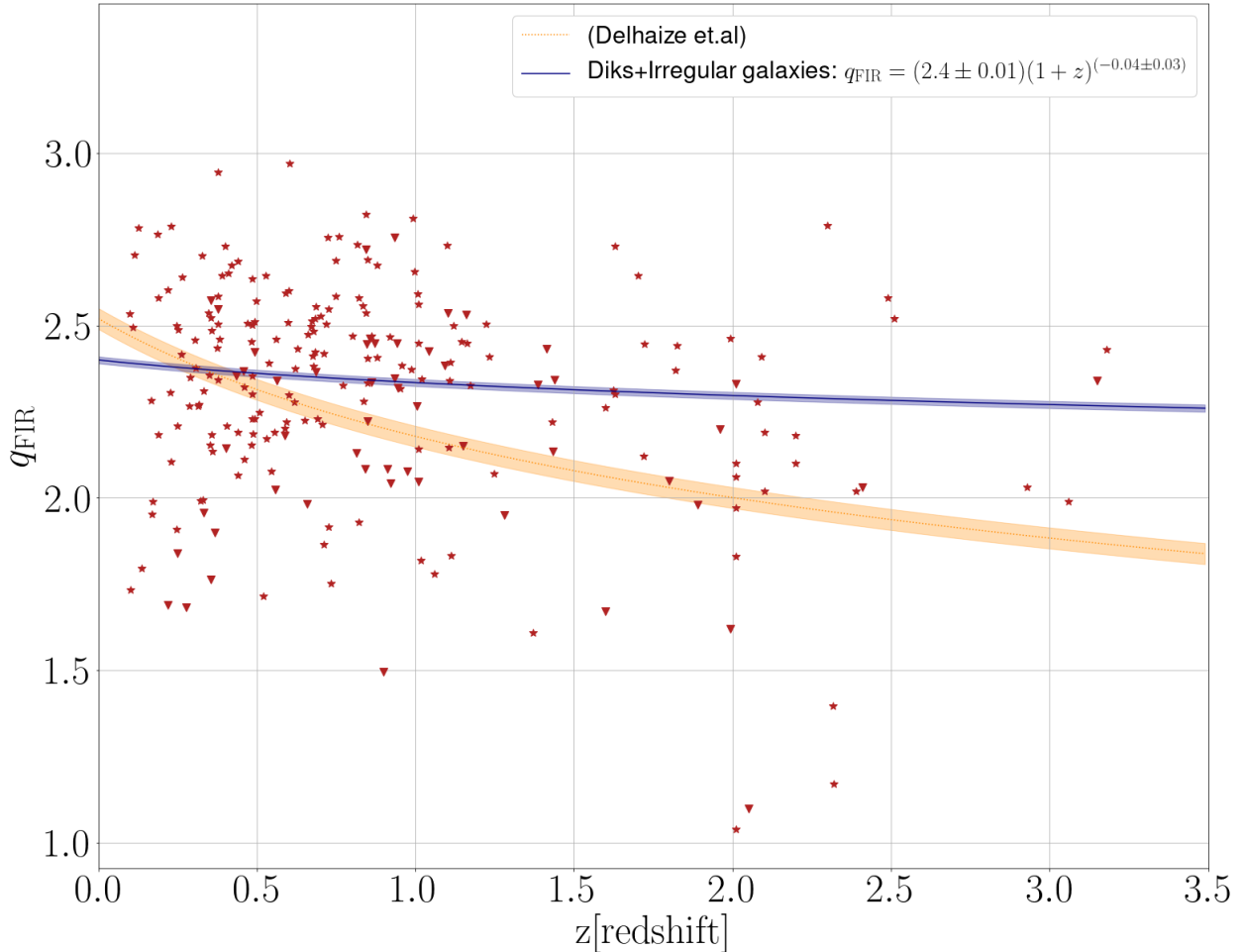
Fig. 4: q_{FIR} versus redshift for 236 SMGs. Red stars represent disk galaxies while red triangles are irregular galaxies. The blue solid curve shows a power-law fit for the whole sample of 236 SMGs (disk + irregular) galaxies. The orange dotted curve is the same power-law fit found in (Delhaize et al. 2017).

an increase in non-thermal radio emission, i.e. the reduction of the correlation parameter. This may, perhaps, explain the results of Delvecchio et al. (2021), which will be the subject of our future analysis.

5. DISCUSSION AND CONCLUSION

Empirically determined correlations have proven to be an excellent tool for studying galaxies at high redshifts, including the FAR-infrared radio correlation. However, recent observations of the star-forming galaxies up to the redshift $z < 6$ have shown that this correlation is evolving with a redshift as $q_{\mathrm{FIR}}(z) = (2.52 \pm 0.03)(1 + z)^{(-0.21 \pm 0.01)}$ (Delhaize et al. 2017). To use this correlation as one of the powerful tools for studying the young universe, we need to understand which physical processes are responsible for this behavior.

Inspired by the work Pavlović et al. (2019), where it was shown that there is an indication that the

evolution of correlation is driven by interactions between galaxies, and the fact that collisions between galaxies can produce an acceleration of cosmic-rays (Lisenfeld and Völk 1993, Murphy 2013, Donevski and Prodanović 2015), in this paper a more detailed analysis of work Pavlović et al. (2019) is done and the dependence of the correlation parameter on the redshift is investigated on a larger sample for different morphology of galaxies. To do so, almost an order of magnitude larger COSMOS sample of 236 star-forming galaxies are taken and based on the three morphological catalogs available for this sample, and the galaxies are divided into 181 disks and 55 irregulars. For both subsamples, the dependence of the correlation parameter on the redshift is examined and the following results are obtained: $q_{\mathrm{FIR}}(z) = (2.4 \pm 0.01)(1 + z)^{(-0.05 \pm 0.04)}$ and $q_{\mathrm{FIR}}(z) = (2.2 \pm 0.1)(1 + z)^{(0.04 \pm 0.08)}$ for disk and irregular galaxies, respectively. None of the subsamples showed any evolution of correlation with the redshift,

nor when the whole sample of 236 galaxies was analyzed, where I obtained: $q_{\mathrm{FIR}}(z) = (2.4 \pm 0.01)(1 + z)^{(-0.04 \pm 0.03)}$. The obtained trends do not show the evolution of correlation and are not consistent with the previously confirmed evolution of the correlation Delhaize et al. (2017). This result is also inconsistent with the results found by Molnár et al. (2018), where it was found that in the sample of spheroid-dominated galaxies there is an evolution of the correlation with the redshift where the b parameter was found to be $b = -0.19 \pm 0.01$. This discrepancy can be explained by the difference in determining the morphology. Namely, in the paper Molnár et al. (2018) the sample of spheroid-dominated galaxies consists of earl-type + disk galaxies with a prominent bulge component, while in our sample of disk galaxies there are only disk-dominated galaxies, while we excluded elliptical galaxies from the analysis. This could mean that active elliptical galaxies (Fukugita et al. 2004, Huang and Gu 2009) are responsible for the evolution of the redshift correlation, which will be the subject of our future research, and which would indicate that whatever the driving mechanism is it is not tightly related to star-formation or gas mass. It is interesting to point out that the mean value of the correlation parameter in irregular galaxies is lower than in disk galaxies. As the sample is dominated by disk galaxies, which is partly consistent with our previous work Pavlović et al. (2019), it is still possible that the different morphology of galaxies drives the evolution of the correlation with the redshift. The result is also consistent with the work of Algera et al. (2020) where it was found that, in the range $1.5 < z < 4$, the mean value of the parameter $q_{\mathrm{FIR}} = 2.2 \pm 0.03$, which is 0.4 dex lower than the local value for a heterogeneous mix of star-forming galaxies (Bell 2003) and ULIRGs (Yun et al. 2001). They interpret the offset concerning the FIRC correlation of normal galaxies through strong magnetic fields in SMGs, combined with the production of secondary cosmic rays, both of which serve to increase the radio output of a galaxy for a given star formation rate, which again supports the hypothesis that an additional population of tidal cosmic rays is responsible for the evolution of FIRC with a redshift. I would like to caution the reader that the parameters now used to determine the morphology of galaxies which are relying on optical images, are not entirely reliable for the redshift $z > 1$. There is a possibility that the subsamples are not completely morphologically clean beyond this redshift, which would significantly affect the results. For this reason, one of the important goals that can emerge from this analysis is to find a new more precise parameter for determining the stage of galaxy collisions at high redshifts, because, as Donevski and Prodanović (2015) have found, the correlation parameter will evolve over the interaction stage. Finally, it is essential to note that we saw that the parameter $q_{\mathrm{FIR}} \sim (1 + z)^{\alpha}$ is very sensitive to the radio spectral index, so there is a possibility that this parameter, i.e. taking it constant, is responsible for the apparent evolution of the correlation, and this will be investigated in the follow-up work.

Table 2: Data sample, colums are as follow: α and δ are the right assension and declination of the object, respectively, z-redshift, S_{FIR}-rest frame FIR flux density from 42 μm to 122 μm in μJy, dS_{FIR}-propagated error on the rest frame FIR flux density, $S_{3\mathrm{GHz}}$- the rest frame 3 GHz flux density in μJy, $dS_{3\mathrm{GHz}}$-integrated error on the 3 GHz flux density, q_{FIR}-correlation parameter, and dq_{FIR}-propagated error on the correlation parameter.

α [°]	δ [°]	z	S_{FIR} [μJy]	dS_{FIR} [μJy]	$S_{3\mathrm{GHz}}$ [μJy]	$dS_{3\mathrm{GHz}}$ [μJy]	q_{FIR}	dq_{FIR}
150.55	1.91	0.55	8897.51	1064.62	0.09	0.02	2.08	0.09
150.62	1.99	1.11	7645.89	1153.42	0.08	0.02	2.15	0.12
150.15	1.80	1.10	15175.45	1111.73	0.05	0.02	2.73	0.18
150.17	2.30	0.44	7465.10	1257.03	0.06	0.01	2.19	0.10
149.54	2.04	0.73	7597.60	215.16	0.17	0.02	1.75	0.05
149.57	1.88	0.62	10836.59	1361.42	0.07	0.02	2.28	0.11
149.57	1.74	0.49	21133.21	5212.18	0.15	0.02	2.23	0.12
149.94	2.67	0.49	18064.39	1689.16	0.13	0.01	2.23	0.06
149.68	2.76	1.11	23428.80	3494.37	0.46	0.02	1.83	0.07
149.68	2.43	0.33	11824.62	1225.23	0.14	0.02	1.99	0.07
149.69	1.67	0.32	27954.73	494.45	0.29	0.05	1.99	0.08
150.75	2.05	0.59	35901.06	2228.78	0.27	0.05	2.20	0.09
150.75	2.36	0.19	40714.40	1547.93	0.12	0.02	2.58	0.07
149.71	2.22	2.32	7563.43	958.31	0.38	0.05	1.40	0.08

Table 2: continued.

α [°]	δ [°]	z	S_{FIR} [μJy]	dS_{FIR} [μJy]	$S_{3\mathrm{GHz}}$ [μJy]	$dS_{3\mathrm{GHz}}$ [μJy]	q_{FIR}	dq_{FIR}
149.92	2.25	1.63	10006.35	1093.49	0.07	0.01	2.31	0.09
149.93	2.30	1.83	13858.89	1367.27	0.08	0.01	2.44	0.08
150.27	2.21	0.85	11435.70	1361.31	0.06	0.01	2.40	0.10
150.28	2.05	1.11	8685.78	356.41	0.06	0.01	2.34	0.10
149.76	2.34	1.01	11590.02	1565.86	0.10	0.01	2.14	0.08
149.77	2.53	0.73	8371.22	558.37	0.13	0.02	1.92	0.06
149.77	2.22	1.60	11521.95	2942.53	0.10	0.01	2.26	0.12
150.46	2.06	0.33	11556.97	4610.53	0.07	0.01	2.31	0.19
150.00	1.94	0.69	13481.89	188.99	0.10	0.01	2.23	0.05
150.00	2.27	0.68	21124.55	452.50	0.08	0.01	2.52	0.06
150.39	2.78	0.36	14194.28	1324.96	0.10	0.02	2.18	0.09
150.44	2.64	0.11	40951.97	3040.25	0.14	0.02	2.50	0.07
149.79	2.29	0.52	5590.52	4378.90	0.13	0.01	1.71	0.34
149.79	2.11	0.48	9348.22	1366.52	0.06	0.01	2.19	0.09
149.79	2.01	1.37	8030.00	1072.62	0.32	0.01	1.61	0.06
149.80	2.14	0.36	34628.75	591.05	0.28	0.03	2.14	0.04
149.80	2.38	0.68	15373.55	155.57	0.08	0.01	2.42	0.06
150.36	2.70	0.32	14688.11	531.13	0.07	0.01	2.38	0.08
150.49	2.73	0.23	10380.46	1686.05	0.09	0.02	2.11	0.11
150.40	2.42	0.17	25002.56	3350.44	0.29	0.07	1.95	0.12
150.40	2.79	0.71	18381.28	2167.93	0.31	0.02	1.87	0.06
149.77	2.47	0.60	16284.43	1741.78	0.10	0.01	2.30	0.07
149.83	1.93	1.43	15558.80	886.68	0.13	0.01	2.22	0.05
149.83	2.55	2.08	9245.63	245.27	0.08	0.01	2.28	0.07
149.84	1.64	1.23	16368.70	2435.86	0.10	0.02	2.41	0.12
150.58	1.89	0.41	9828.47	1214.50	0.07	0.02	2.21	0.11
150.65	2.03	0.44	10340.76	856.01	0.11	0.02	2.06	0.09
150.68	2.23	0.59	19893.95	1775.35	0.07	0.02	2.59	0.13
150.69	1.62	1.02	11166.88	832.81	0.22	0.02	1.82	0.06
150.04	2.08	0.46	18798.90	2788.78	0.10	0.01	2.32	0.08
150.21	2.36	0.17	50380.17	5107.55	0.27	0.03	2.28	0.07
150.33	1.92	0.10	72256.35	9819.26	1.37	0.05	1.73	0.06
150.34	2.05	0.85	15191.30	1867.16	0.10	0.01	2.28	0.08
150.30	2.05	0.71	16659.07	1153.81	0.08	0.01	2.42	0.07
149.48	1.86	0.51	30403.79	5883.63	0.21	0.02	2.25	0.09
150.12	2.46	0.25	52507.87	4588.46	0.70	0.03	1.91	0.04
149.74	2.07	0.74	12732.01	798.42	0.06	0.01	2.48	0.11
149.74	2.18	0.35	17565.86	2391.38	0.14	0.02	2.15	0.09
150.27	1.98	1.17	17605.57	1393.13	0.11	0.01	2.33	0.06
150.60	2.45	0.38	20699.26	6254.93	0.08	0.02	2.50	0.16
150.60	2.75	0.65	12267.35	974.19	0.09	0.03	2.22	0.15
150.60	2.12	0.38	15502.48	334.09	0.08	0.02	2.34	0.08
149.85	2.78	0.14	27909.41	5186.01	0.46	0.05	1.80	0.09
149.87	2.16	0.94	10218.45	1086.14	0.07	0.05	2.32	0.35
150.31	2.24	0.25	19858.26	1274.26	0.07	0.01	2.50	0.07
149.91	2.45	0.58	9721.46	391.29	0.08	0.01	2.17	0.07
150.34	2.57	0.82	14557.66	1612.38	0.24	0.01	1.93	0.05
150.11	2.53	1.99	11751.46	1320.59	0.07	0.01	2.46	0.09
149.97	2.54	0.23	23879.13	398.81	0.07	0.01	2.60	0.08
149.98	2.43	0.48	15832.57	1014.17	0.13	0.01	2.15	0.06

Table 2: continued.

α [°]	δ [°]	z	S_{FIR} [μJy]	dS_{FIR} [μJy]	$S_{3\mathrm{GHz}}$ [μJy]	$dS_{3\mathrm{GHz}}$ [μJy]	q_{FIR}	dq_{FIR}
150.17	2.13	0.19	19476.74	2826.56	0.14	0.01	2.18	0.07
150.17	2.48	0.74	15911.69	1552.31	0.07	0.01	2.47	0.09
150.19	2.68	0.29	23701.58	2923.56	0.17	0.02	2.21	0.07
150.19	2.68	0.32	44615.32	433.87	0.27	0.04	2.27	0.06
150.42	2.12	0.67	16478.81	277.80	38.80	2.90	2.53	0.04
149.85	2.32	0.38	11125.89	1109.59	26.60	2.60	2.49	0.07
150.76	2.04	1.01	15940.94	2729.45	48.50	3.60	2.45	0.08
149.72	1.62	0.10	25024.54	3508.42	48.70	3.60	2.53	0.09
149.59	2.40	1.11	11733.85	1045.17	41.40	3.30	2.39	0.05
149.53	2.42	0.49	13682.28	1778.37	23.90	3.10	2.63	0.09
150.58	2.26	0.99	9798.63	114.81	35.20	2.90	2.37	0.04
149.51	2.69	0.26	19251.25	817.14	52.10	3.90	2.42	0.06
149.80	2.12	0.49	10037.61	1092.16	33.50	2.90	2.35	0.07
150.55	2.56	0.60	9732.79	204.50	23.50	2.50	2.51	0.05
150.55	2.49	0.86	12528.88	516.70	35.10	2.90	2.47	0.04
150.48	1.95	0.67	13215.96	434.45	33.30	2.80	2.50	0.04
149.91	2.61	0.35	20341.48	936.44	64.90	4.00	2.36	0.05
150.52	2.53	0.41	11543.54	1134.28	19.00	2.50	2.65	0.08
150.34	1.61	0.23	5229.76	3469.70	18.00	2.70	2.31	0.30
150.62	2.33	0.49	9279.77	614.27	21.60	2.50	2.51	0.07
149.64	2.02	0.36	11307.85	445.80	24.70	2.60	2.52	0.06
150.35	2.40	0.14	35107.66	5068.06	39.10	3.10	2.78	0.09
149.67	1.71	0.38	16180.74	730.70	43.50	3.20	2.43	0.05
149.76	1.99	0.50	15007.69	937.29	30.50	2.80	2.57	0.06
150.50	2.20	1.72	7040.84	269.21	24.30	2.50	2.45	0.05
150.75	2.59	0.69	13257.17	146.55	29.40	3.20	2.55	0.05
149.76	1.87	0.54	14231.01	663.12	44.30	3.30	2.39	0.05
150.29	1.69	1.25	5734.58	327.56	43.50	3.20	2.07	0.04
150.42	1.82	0.85	7631.56	4124.08	29.20	2.70	2.33	0.24
150.37	1.69	1.00	11698.40	1872.48	22.00	2.60	2.66	0.09
149.70	2.61	0.41	15232.03	558.04	23.70	2.70	2.68	0.06
150.24	2.85	0.29	11098.55	396.89	35.40	3.10	2.35	0.06
149.99	2.32	0.85	7097.75	435.71	11.90	2.40	2.69	0.09
150.09	2.43	0.36	15116.15	1352.03	32.00	2.70	2.54	0.07
150.26	2.51	0.17	6490.29	1684.22	45.50	3.20	1.99	0.13
150.69	2.14	0.40	17023.25	65.30	23.30	2.90	2.73	0.07
150.27	2.62	0.67	8364.18	232.16	25.60	2.60	2.41	0.05
149.92	2.31	0.66	5320.67	1635.90	14.10	2.50	2.47	0.16
149.66	2.13	0.56	18451.58	2060.18	49.30	3.60	2.46	0.06
150.11	2.55	0.72	6033.37	2686.97	13.70	2.40	2.55	0.21
149.88	2.07	0.60	15146.36	940.19	12.60	2.30	2.97	0.09
150.60	2.40	0.60	11160.95	1488.41	21.80	2.50	2.60	0.08
149.60	2.23	0.63	11189.69	1213.25	32.30	3.10	2.43	0.07
150.38	2.81	0.23	17305.81	54.22	19.70	2.50	2.79	0.07
149.89	2.47	0.71	6712.19	91.77	32.80	2.80	2.21	0.04
150.72	1.72	0.30	17648.06	2316.76	43.90	3.30	2.46	0.08
150.72	1.77	0.85	14121.47	2479.87	33.80	3.20	2.54	0.09
150.54	2.53	0.62	8549.51	1901.59	28.10	2.70	2.38	0.11
150.48	2.61	0.11	19114.78	883.71	25.30	2.60	2.70	0.07
150.49	2.67	0.72	13037.04	429.65	18.30	2.40	2.76	0.06

Table 2: continued.

α [°]	δ [°]	z	$S_{\rm FIR}$ [μJy]	$dS_{\rm FIR}$ [μJy]	$S_{\rm 3GHz}$ [μJy]	$dS_{\rm 3GHz}$ [μJy]	$q_{\rm FIR}$	$dq_{\rm FIR}$
150.52	2.20	0.38	11942.51	591.55	22.70	2.60	2.58	0.07
149.56	2.35	1.12	5612.45	912.01	15.50	2.80	2.50	0.11
150.11	1.67	0.48	17770.78	1070.39	47.00	3.30	2.45	0.05
150.62	2.53	0.32	5642.59	694.03	21.70	2.60	2.27	0.09
150.17	2.36	0.67	11056.67	783.79	26.80	2.70	2.51	0.06
150.05	2.70	0.82	9032.05	729.88	13.60	2.40	2.74	0.09
150.06	1.68	0.53	10506.25	1203.03	18.20	2.50	2.64	0.08
150.51	2.78	0.33	14249.11	1656.85	20.30	2.40	2.70	0.08
150.00	2.30	0.50	7949.58	245.49	12.40	2.40	2.69	0.09
150.56	2.36	0.99	8899.86	1927.69	11.70	2.40	2.81	0.13
150.33	1.87	0.82	10791.62	40.90	23.30	2.60	2.58	0.05
150.56	2.46	0.27	8026.83	2033.04	13.00	2.30	2.64	0.14
150.57	2.21	0.75	8069.05	1116.79	16.90	2.60	2.59	0.09
149.57	1.62	0.45	10678.65	754.61	61.50	4.10	2.11	0.05
149.57	2.63	0.27	10311.38	1217.29	39.50	3.10	2.27	0.08
150.24	2.32	0.38	20339.61	5267.57	16.90	2.50	2.94	0.13
150.07	2.23	0.19	24557.85	843.70	29.10	2.70	2.76	0.07
150.43	2.28	0.49	11645.26	11732.95	27.60	2.70	2.50	0.44
150.69	1.74	0.25	17838.55	2407.29	40.70	3.20	2.49	0.08
150.40	2.67	0.49	9758.70	649.36	22.90	2.70	2.51	0.07
150.41	2.43	0.39	9560.16	2546.71	15.90	2.40	2.64	0.14
149.51	2.63	0.72	5929.76	1000.38	14.90	2.80	2.50	0.11
150.18	2.29	0.73	7229.35	10.04	11.90	2.30	2.69	0.09
150.26	1.94	0.68	7054.28	33.37	23.20	2.60	2.38	0.05
150.59	2.41	1.15	12320.46	5359.75	38.00	3.00	2.45	0.19
149.59	2.24	0.56	2805.62	1819.50	13.90	2.60	2.19	0.29
149.78	2.27	1.22	7135.15	290.90	19.90	2.50	2.50	0.06
150.55	1.64	0.49	9879.97	77.24	37.30	3.10	2.30	0.05
150.35	2.72	0.38	11538.42	1921.58	29.20	2.80	2.46	0.09
150.17	1.81	0.85	15501.34	2146.64	19.20	2.50	2.82	0.08
150.65	2.70	0.59	5576.31	346.45	26.10	2.70	2.22	0.06
150.65	2.00	1.01	6795.39	887.12	14.80	2.50	2.59	0.09
150.32	2.27	0.80	7746.95	858.08	29.80	2.70	2.33	0.06
149.82	2.42	0.84	5397.73	555.18	12.30	2.30	2.56	0.09
150.28	1.78	0.88	3780.02	107.50	12.30	2.40	2.41	0.09
149.50	2.18	1.02	7747.63	3.71	30.00	3.50	2.34	0.05
150.68	2.62	0.92	8855.81	498.89	25.30	2.80	2.47	0.05
149.88	2.77	0.76	8300.71	49.69	11.70	2.40	2.76	0.09
149.72	2.71	0.88	11803.85	18.22	20.70	2.60	2.67	0.06
149.58	2.52	1.16	10207.11	4.17	31.90	2.90	2.45	0.04
150.55	1.81	1.01	6154.37	135.18	14.40	2.40	2.56	0.07
150.07	2.07	0.96	7401.31	327.50	25.80	2.60	2.38	0.05
149.50	2.49	1.70	8381.65	465.83	18.30	2.90	2.64	0.08

REFERENCES

Algera, H. S. B., Smail, I., Dudzevičiūtė, U., et al. 2020, ApJ, 903, 138

Aretxaga, I., Wilson, G. W., Aguilar, E., et al. 2011, Monthly Notices of the Royal Astronomical Society, 415, 3831

Bell, E. F. 2003, ApJ, 586, 794

Bertone, S. and Conselice, C. J. 2009, MNRAS, 396, 2345

Casey, C. M., Narayanan, D. and Cooray, A. 2014, PhR, 541, 45

Cassata, P., Guzzo, L., Franceschini, A., et al. 2007, ApJS, 172, 270

Chiosi, C. and Carraro, G. 2002, MNRAS, 335, 335

Civano, F., Elvis, M., Brusa, M., et al. 2012, in VizieR Online Data Catalog (VizieR Online Data Catalog), J/ApJS/201/30

Civano, F., Marchesi, S., Comastri, A., et al. 2016, in VizieR Online Data Catalog (VizieR Online Data Catalog), J/ApJ/819/62

Condon, J. J. 1992, ARA&A, 30, 575

Condon, J. J., Anderson, M. L. and Helou, G. 1991, ApJ, 376, 95

Conselice, C. J. 2007, in Galaxy Evolution across the Hubble Time, ed. F. Combes and J. Palouš, Vol. 235, 381–384

Conselice, C. J., Yang, C. and Bluck, A. F. L. 2009, MNRAS, 394, 1956

Croom, S. M., Smith, R. J., Boyle, B. J., et al. 2001, MNRAS, 322, L29

Croom, S. M., Smith, R. J., Boyle, B. J., et al. 2004, MNRAS, 349, 1397

De Lucia, G., Springel, V., White, S. D. M., Croton, D. and Kauffmann, G. 2006, MNRAS, 366, 499

Del Moro, A., Alexander, D. M., Mullaney, J. R., et al. 2013, A&A, 549, A59

Delhaize, J., Smolčić, V., Delvecchio, I., et al. 2017, A&A, 602, A4

Delvecchio, I., Gruppioni, C., Pozzi, F., et al. 2014, MNRAS, 439, 2736

Delvecchio, I., Smolčić, V., Zamorani, G., et al. 2017, A&A, 602, A3

Delvecchio, I., Daddi, E., Sargent, M. T., et al. 2021, A&A, 647, A123

Donevski, D. and Prodanović, T. 2015, MNRAS, 453, 638

Donevski, D., Buat, V., Boone, F., et al. 2018, A&A, 614, A33

Donley, J. L., Rieke, G. H., Rigby, J. R. and Pérez-González, P. G. 2005, ApJ, 634, 169

Donley, J. L., Koekemoer, A. M., Brusa, M., et al. 2012, ApJ, 748, 142

Elvis, M., Civano, F., Vignali, C., et al. 2009, ApJS, 184, 158

Ezawa, H., Kawabe, R., Kohno, K. and Yamamoto, S. 2004, in Society of Photo-Optical Instrumentation Engineers (SPIE) Conference Series, Vol. 5489, Ground-based Telescopes, ed. J. Oschmann, Jacobus M., 763–772

Fukugita, M., Nakamura, O., Turner, E. L., Helmboldt, J. and Nichol, R. C. 2004, ApJL, 601, L127

Gürkan, G., Hardcastle, M. J., Smith, D. J. B., et al. 2018, MNRAS, 475, 3010

Helou, G., Soifer, B. T. and Rowan-Robinson, M. 1985, ApJL, 298, L7

Huang, S. and Gu, Q. S. 2009, MNRAS, 398, 1651

Hurley, P. D., Oliver, S., Betancourt, M., et al. 2017, MNRAS, 464, 885

Klein, U., Lisenfeld, U. and Verley, S. 2018, A&A, 611, A55

Kotarba, H., Karl, S. J., Naab, T., et al. 2010, ApJ, 716, 1438

Laigle, C., McCracken, H. J., Ilbert, O., et al. 2016, ApJS, 224, 24

Le Fèvre, O., Tasca, L. A. M., Cassata, P., et al. 2015, A&A, 576, A79

Lilly, S. J., Le Fèvre, O., Renzini, A., et al. 2007, ApJS, 172, 70

Lisenfeld, U. and Völk, H. J. 1993, in Star Formation, Galaxies and the Interstellar Medium, 76

Lutz, D., Poglitsch, A., Altieri, B., et al. 2011, A&A, 532, A90

Magnelli, B., Lutz, D., Berta, S., et al. 2010, A&A, 518, L28

Magnelli, B., Ivison, R. J., Lutz, D., et al. 2015, A&A, 573, A45

Marchesi, S., Civano, F., Elvis, M., et al. 2016, ApJ, 817, 34

Miettinen, O., Delvecchio, I., Smolčić, V., et al. 2017, A&A, 606, A17

Molnár, D. C., Sargent, M. T., Delhaize, J., et al. 2018, MNRAS, 475, 827

Mortlock, A., Conselice, C. J., Hartley, W. G., et al. 2013, MNRAS, 433, 1185

Mundy, C. J., Conselice, C. J., Duncan, K. J., et al. 2017, MNRAS, 470, 3507

Murphy, E. J. 2013, ApJ, 777, 58

Murphy, E. J., Bremseth, J., Mason, B. S., et al. 2012, ApJ, 761, 97

Norris, R. P., Afonso, J., Appleton, P. N., et al. 2006, AJ, 132, 2409

Oliver, S. J., Bock, J., Altieri, B., et al. 2012, Monthly Notices of the Royal Astronomical Society, 424, 1614

Park, S. Q., Barmby, P., Fazio, G. G., et al. 2008, ApJ, 678, 744

Pavlović, M. and Prodanović, T. 2019, MNRAS, 489, 4557

Pearson, W. J., Wang, L., van der Tak, F. F. S., et al. 2017, A&A, 603, A102

Pilbratt, G. L., Riedinger, J. R., Passvogel, T., et al. 2010, A&A, 518, L1

Prodanović, T., Bogdanović, T. and Urošević, D. 2013, PhRvD, 87, 103014

Sajina, A., Yan, L., Lutz, D., et al. 2008, ApJ, 683, 659

Sargent, M. T., Carollo, C. M., Lilly, S. J., et al. 2007, ApJS, 172, 434

Sargent, M. T., Schinnerer, E., Murphy, E., et al. 2010, ApJL, 714, L190

Scarlata, C., Carollo, C. M., Lilly, S., et al. 2007, ApJS, 172, 406

Schinnerer, E., Sargent, M. T., Bondi, M., et al. 2010, in VizieR Online Data Catalog (VizieR Online Data Catalog), J/ApJS/188/384

Smolčić, V., Delvecchio, I., Zamorani, G., et al. 2017a, A&A, 602, A2

Smolčić, V., Novak, M., Bondi, M., et al. 2017b, A&A, 602, A1

Tasca, L. A. M., Kneib, J. P., Iovino, A., et al. 2009, A&A, 503, 379

Tasca, L. A. M., Le Fèvre, O., Ribeiro, B., et al. 2017, A&A, 600, A110

van der Kruit, P. C. 1971, A&A, 15, 110

Ventou, E., Contini, T., Bouché, N., et al. 2017, A&A, 608, A9

Wang, T. 2019, in ALMA2019: Science Results and Cross-Facility Synergies, 6

Yun, M. S., Reddy, N. A. and Condon, J. J. 2001, ApJ, 554, 803

ДА ЛИ ДАЛЕКА ИНФРАЦРВЕНА-РАДИО КОРЕЛАЦИЈА ЕВОЛУИРА СА ЦРВЕНИМ ПОМАКОМ КОД НЕПРАВИЛНИХ И ДИСКОЛИКИХ ГАЛАКСИЈА?

M. S. Pavlović[1,2]

[1]*Mathematical institute of the Serbian Academy of Sciences and Arts*
Kneza Mihaila 36, 11000 Belgrade, Serbia

[2]*Faculty of Mathematics, Department of Astronomy, University of Belgrade*
Studentski Trg 16, 11000 Belgrade, Serbia

E–mail: *marinap@mi.sanu.ac.rs*

Потврђено да постоји јака линеарна зависност између термалног инфрацрвеног зрачења и нетермалног радио-зрачења код галаксија у којима се формирају звезде. Скорашњи радови који су се заснивали на проучавању ове корелације на великим црвеним помацима, показали су еволуцију параметра корелације. У овом раду, истражићу могуће физичке процесе који су заслужни за ову еволуцију. Један могући узрок оваквог понашања корелације јесте интеракција између галаксија. Користила сам морфологију галаксија као индикатор прошле и садашње интеракције, јер је опште познато да неправилне галаксије настају сударима или блиским пролазима. Да бих тестирала ову хипотезу, узела сам узорак галаксија у субмилиметарском подручју до црвеног помака $z = 3.5$ из поља COSMOS. У односу на морфолошки тип, узорак је подељен на два подузорка (дисколике и неправилне галаксије), а еволуција корелације је испитана код оба подузорка засебно. Показано је да код оба подузорка не постоји индикација за еволуцију далеке инфрацрвене-радио корелације са црвеним помаком. Међутим, пронађено је да је средња вредност параметра корелације нижа код неправилних галаксија, што може да утиче на еволуцију корелације, ако се број неправилних галаксија повећава са црвеним помаком. Дисколике галаксије, које доминирају овим узорком могу бити заслужне за привидни недостатак ове еволуције. Са друге стране, постоји велики проблем код оптичког одређивања морфологије галаксија на великим црвеним помацима због непрозрачности прашине. Да би се тестирала хипотеза да су галаксије у интеракцији заслужне за еволуцију корелације са црвеним помаком, потребно је да се анализира много већи узорак галаксија чија морфологија је одређена помоћу слика добијених са телескопа VLA и ALMA, као додатак оптичким сликама. Коначно, пронађено је да је параметар q_{FIR}, а самим тим и еволуција корелације, веома осетљив на радио-спектрални индекс, те узимање константне вредности овог параметра може бити заслужно за посматрану еволуцију корелације.